JPhys Photonics

Subwavelength phase engineering deep inside silicon

Journal of Physics: Photonics

PAPER

Subwavelength phase engineering deep inside silicon

Mehmet Bütün[1], **Alperen Saltik**[1] and **Onur Tokel**[1,2,*]

[1] Department of Physics, Bilkent University, Ankara, Turkey
[2] National Nanotechnology Research Center and Institute of Materials Science and Nanotechnology, Bilkent University, Ankara, Turkey
* Author to whom any correspondence should be addressed.

E-mail: otokel@bilkent.edu.tr

Keywords: in-chip, silicon photonics, metaoptics, laser writing, optical lithography

Supplementary material for this article is available online

OPEN ACCESS

RECEIVED
7 May 2025

REVISED
19 July 2025

ACCEPTED FOR PUBLICATION
5 August 2025

PUBLISHED
20 August 2025

Abstract

Recent advances in three-dimensional laser writing have enabled direct nanostructuring deep within silicon, unlocking a volumetric design space previously inaccessible to surface-bound nanophotonic devices. Here, we introduce subwavelength phase engineering inside crystalline silicon, offering a novel strategy for integrated photonics. We design and numerically demonstrate a volumetric metaoptic monolithically embedded within the bulk, achieving full 2π phase control at telecommunication wavelengths, with simulated transmission efficiencies reaching 90%. The architecture is guided by a semi-analytical Fabry–Pérot model and validated through full-wave simulations. Arrays of 250 nm-wide metaatoms spaced at 300–410 nm pitch yield a focusing efficiency of 70%. With the wafer surface left pristine, this platform can potentially enable co-integration with electronics, MEMS/NEMS, and conventional metasurfaces. Moreover, the method is directly transferable to other transparent dielectrics compatible with ultrafast laser writing. These results establish a CMOS-compatible blueprint for three-dimensional nanophotonics and multi-level integration within the wafer.

1. Introduction

Silicon (Si) is a foundational material in electronics, photovoltaics and Si-photonics, where planar nanolithography is routinely employed to sculpt state-of-the-art nanophotonic devices on the wafer surface [1]. Exploiting the bulk of Si, rather than its surface, would unlock a fundamentally different platform for optical control [2]. Three-dimensional (3D) nonlinear laser lithography offers a direct and mask-free approach to functionalize the wafer interior [3–5]. These in-chip or in-volume techniques harness nonlinear absorption of laser pulses and their feedback-driven interactions to induce structural modifications deep within the crystal [3–5], enabling precise volumetric patterning [3, 6–8]. Importantly, this process preserves the wafer surface, allowing compatibility with existing device integration strategies [3].

The laser-written regions inside Si have already enabled a range of volumetric photonic components, including waveguides, lenses, gratings, waveplates, and both Fourier and Fresnel holograms along with applications in optical data storage [3, 5, 9–16]. The emerging depth dimension has also been shown to boost the efficiency of micro-optics. For instance, the efficiency of diffraction gratings is significantly improved with effective field enhancement achieved over a 3D optical lattice formed inside the wafer [15]. Such an improvement would not be possible with single-level fabrication [15]. While these exciting advances have focused on micro-structuring, the recent discovery of volumetric nano-fabrication in Si is envisioned to enable nanophotonics or metaoptics capabilities directly inside the wafer [17]. In order to realize this potential and guide the next generation of experiments, it is essential to develop optical architectures that are inherently compatible with the depth degree-of-freedom.

Metamaterials, composed of subwavelength building blocks known as metaatoms, [18, 19] would be appropriately challenging to create with in-chip approaches. The metaatoms are engineered to manipulate electromagnetic waves for advanced functionality [20]. Due to the numerous challenges in 3D fabrication, the field focuses on metasurfaces. These are more practical, as they require two-dimensional patterning with

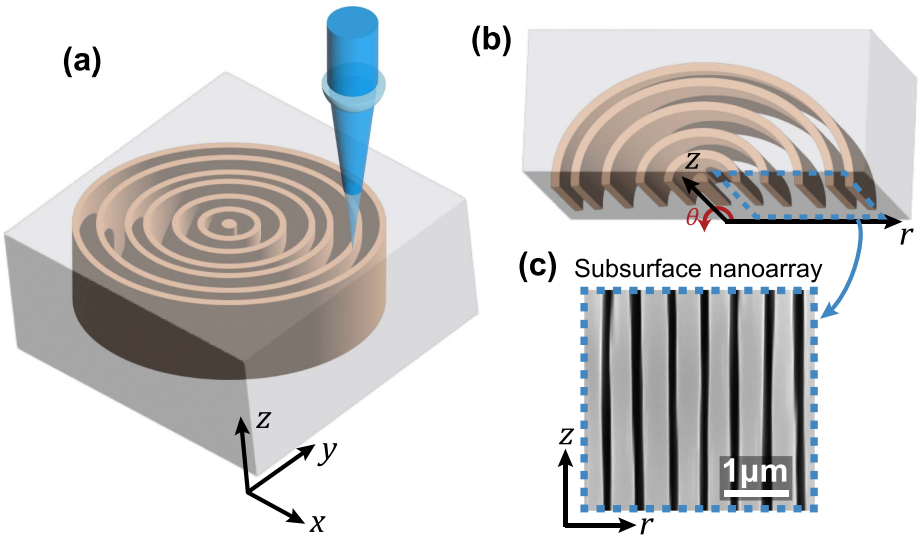

Figure 1. The concept of in-chip metaoptics. (a) Using three-dimensional laser writing, subsurface patterns with subwavelength features are created deep inside Si. Metaatoms are designed to create a particular phase pattern, enabling plug-and-play functionality. (b) A representative metalens inside Si. These may also be integrated with conventional metasurfaces. (c) Scanning electron microscopy image of a cross-section of the direct-laser-written nano-structures buried inside silicon. The sample is etched briefly, revealing a regular array with a feature size of 154 ± 20 nm and a period of 611 ± 47 nm. A ns-pulsed laser of 1.55 μm wavelength, 5 μJ pulse energy, linear polarization, and Bessel-profile is used.

subwavelength resolution and pitch [21, 22]. In contrast, 3D laser nano-fabrication is uniquely suitable to exploit the bulk [17].

Although early developments in metaoptics focused on metallic resonators [23], recent efforts have shifted toward dielectric materials such as Si, which offer high refractive index contrasts and low optical losses [24–27]. These devices have been adopted for numerous functionalities, with control over the phase, amplitude, and polarization of light [28–30]. Common metasurface implementations include arrays of nanopillars patterned on planar substrates [29, 31, 32], or alternatively, subwavelength holes with varying diameters etched into a host material [28, 33]. The optical response is governed by the height, pitch, and geometry of these nanostructures, facilitating enhanced light–matter interaction and advanced optics such as flat lenses [30, 33]. Despite significant progress, such metaoptics remain confined to surface-bound architectures, with their practical deployment hindered by complex nanofabrication demands, structural fragility, and susceptibility to environmental exposure [34].

In this work, we introduce a design paradigm that leverages the volumetric nature of laser writing [17] to enable monolithic, buried metaoptics compatible with conventional Si-photonics and metasurface platforms. By relocating optical functionality from the surface to the interior, this strategy mitigates contamination and packaging constraints while introducing a previously inaccessible integration dimension. Specifically, we present a framework for subwavelength phase engineering deep inside Si. Continuous tiling of resonant metaatoms enables the construction of a hyperbolic-phase metalens with an aperture of 100 μm and a focal length of 120 μm. Simulations predict full 2π phase coverage, up to 90% transmission for individual metaatoms, and a focusing efficiency of 70% at the wavelength of 1.55 μm.

These results establish a foundation for extending metaoptics into the bulk of crystalline Si and, more broadly, for enabling multi-level 3D photonic integration in semiconductor platforms through in-chip fabrication.

We build on the emerging foundation of in-chip laser nanostructuring, aiming for a design compatible with current subsurface fabrication capabilities (figure 1) [17]. State-of-the-art laser writing in Si has achieved resolutions down to 100 nm and pitch values as low as 300 nm [17]. We show that optical functionality emerges from light interacting with such laser-written nanostructures, with phase shifts computed using finite-difference time-domain (FDTD) simulations across a range of pitch and height values. Our target is full 2π phase modulation for advanced wavefront control. Based on these simulations, we design and numerically evaluate a subsurface metalens (figures 1(a) and (b)). The required feature sizes and periodic nanopatterning fall within the capabilities of current experimental techniques across various contexts. As a proof of principle, we fabricate buried nanoarrays inside Si with laser pulses of $\varepsilon_p = 5\,\mu J$, linear polarization, and Bessel-type beam profile (figure 1(c)). The fabrication and characterization procedures of

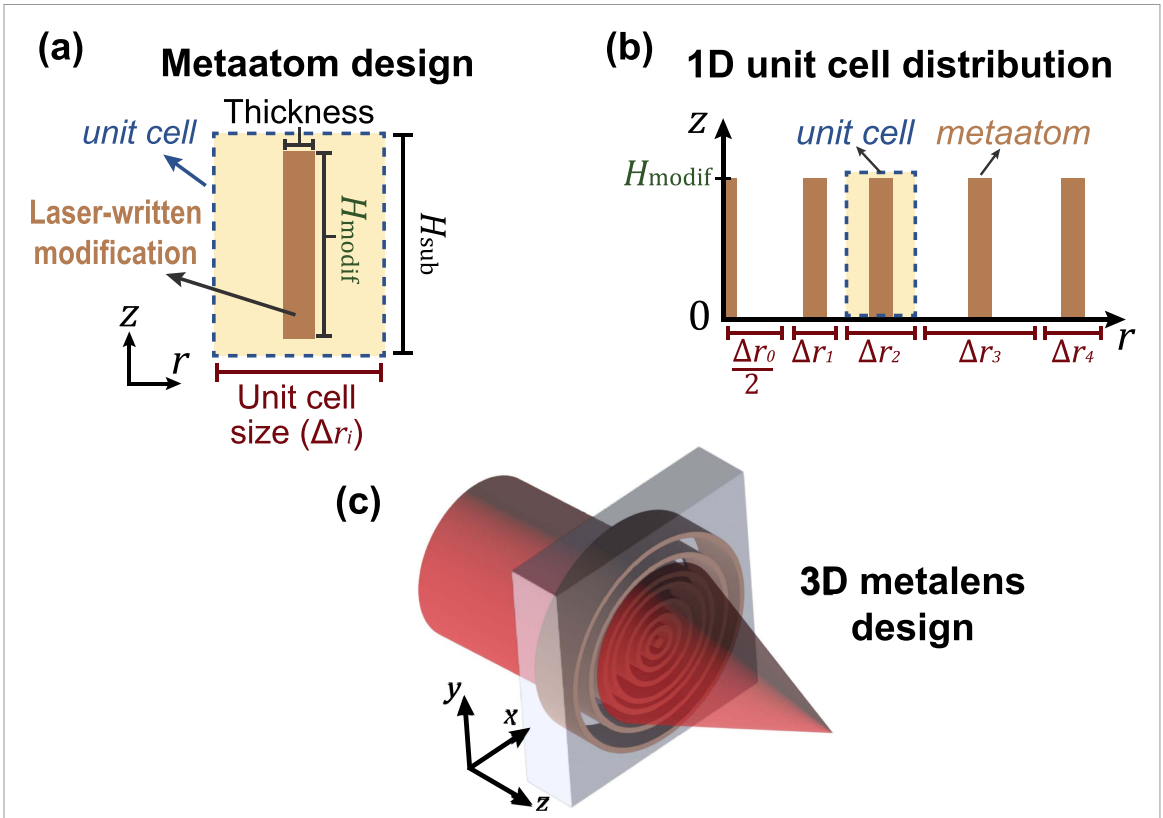

Figure 2. Metaoptics buried inside Si. (a) The metaatoms and unit cells from the crosssection of 3D optics. Metaatom width is (δl) assumed to be small enough to consider them as rectangular prisms with thickness of $\zeta = 250$ nm and height H_{modif}. (b) Metaatom distribution over the r coordinate. The unit cell (Δr_i) and patterning over r are selected based on the targeted phase map of the lens. (c) 3D metalens is formed by continuous tiling of the pattern in (b) over the azimuthal angle (θ), resulting in slightly elliptical forms.

nanopatterns are detailed in the supplementary Methods and in [17]. Scanning electron microscope (SEM) analysis reveals periodic buried structures with feature size of 154 ± 20 nm and a pitch of 611 ± 47 nm (figure 1(c)). These results highlight the feasibility of high-aspect-ratio periodic nanostructuring in Si. Our simulations further demonstrate their optical potential in 3D nano-engineering. We conclude with a discussion of current limitations and future directions toward the realization of 3D Si-nanophotonics.

2. Design of subsurface metaatoms

Metasurfaces consist of basic units, *i.e.*, metaatoms, engineered to impart complex optical functionality [29, 30]. Here we pursue a distinct paradigm in which the metaatoms are buried within crystalline Si. In contrast to conventional surface-bound fabrication schemes [28], our approach relies on direct laser writing [17]. A novel seeding-based mechanism enables subwavelength features with aspect ratios (>1000) and allows multilevel nanostructuring deep inside Si [17]. Accordingly, each metaatom is modeled as a laser-written structure of thickness ζ and height H_{modif} embedded in the crystal (figure 2(a)). The lateral position, depth, feature size, and unit-cell geometry of the patterns can be controlled using holographic structuring and beam positioning techniques [17]. This freedom already allows diverse design options, e.g. high-efficiency volume nano-gratings [17].

The unit cells are to be tiled over a volume resulting in the novel architecture (figures 2(b) and (c)). The tiling pattern and feature dimensions are selected according to the target wavelength and desired optical functionality. We adopt the pitch as the control parameter for phase, as it can be adjusted in experiments. In order to create the circular symmetry of a lens, we exploit continuous laser-written arrays. This is a unique feature of laser-writing inside Si [17]. In our preliminary experiments, we find that it is possible to fabricate continuous as well as curved nano-structures inside Si. The resulting pattern (figure 2(c)) resembles a Fresnel lens, however, the operating principles are distinct. The former is based on Fourier optics, whereas our device exploits resonant coupling of wavelength-scale metaatoms [35].

The optical index landscape for laser-modified Si is evolving rapidly, and remains a challenge to pin down quantitatively. Currently the index contrast is modest at the nanoscale ($|\Delta n| \approx 10^{-2}$) [17]. Closer

Table 1. Metaatom design parameters.

Properties	Values
Material	Silicon
Wavelength	$\lambda = 1550\,\text{nm}$
Wavelength in medium	$\lambda_{\text{Si}} = 445\,\text{nm}$
Modification thickness	$\zeta = 250\,\text{nm}$
Substrate height	$H_{\text{sub}} = 80 \times \lambda_{\text{Si}}$ (35.63 μm)
Modification height	$H_{\text{modif}} = 60 \times \lambda_{\text{Si}}$ (26.72 μm)
Refractive index contrast	$\Delta n = 0.25$

structural analyses, however, reveal two distinct microphases, localized amorphous pockets and nanovoids, that substantially broaden the attainable index range [2, 17, 36]. The amorphous phase supports $\Delta n \approx +0.25$, while void formation can yield $\Delta n \approx -2.5$ [17, 37]. Indeed, ultrafast-pulse studies in Si already achieved partial amorphization with $\Delta n \approx +0.1$ [38]. Moreover, tailoring the pulse width permits access to both positive [36, 39, 40], and negative-contrast regimes [2, 41]. A complementary route exploits the discovery of stress-induced birefringence to fabricate the first waveplates embedded in Si [5]. Taken together, these results indicate that laser-based refractive-index engineering offers a path forward, and we presume controlled amorphization may be achieved with refined techniques [3, 36, 38]. Thus, we first investigated the case of $\Delta n = 0.25$, followed by $|\Delta n| = 10^{-2}$. In both cases, we find full 2π phase modulation may be possible, suggesting advanced photonics capabilities through judicious combination of existing features, emerging architectures and refractive index engineering.

3. Theory and simulations

We employ the FDTD method to model both the individual metaatoms and the complete metalens. The optical response of a single metaatom is first obtained with a 2D FDTD solver. In this configuration a linearly-polarized plane wave propagates along the z-axis (figure 2(a)). Periodic boundary conditions are imposed on the r_{min} and r_{max} boundaries, and perfectly matched layers (PMLs) are applied at z_{min}, z_{max} to absorb outgoing waves. The resulting transmission and phase-shift spectra provide the lookup table used in the metalens design. The full device is then analyzed with a 3D FDTD simulation that employs the same PML treatment on all outer boundaries.

The parameters for the first metaatom design are summarized in table 1. All simulations target the near-infrared wavelength $\lambda = 1.55\,\mu$m, well inside the transparency window of Si ($>1\mu$m). Throughout the simulations, the metaatom height ($H_{\text{modif}} = 60\ \lambda_{\text{Si}}$) and thickness ($\zeta = 250$ nm) are held constant, while the phase modulation is recorded as a function of the unit cell size (Δr_i). We sweep Δr_i in the range of 300–500 nm, a range that supports strong resonant coupling, while suppressing higher diffraction orders (figure 3) [42]. FDTD simulations with x-polarized light yield the phase modulation map given in (figure 3(a)), indicating smooth phase control across the selected pitch range. We observe full 2π phase shift modulation (figure 3(c)), with the transmission profile given in (figure 3(d)).

As a secondary approach to ascertain the phase modulation, we developed a semi-analytical model tailored to our geometry. When neighboring metaatoms are closely spaced, the ensemble can be approximated as a homogeneous slab of effective refractive index n_{eff}. In that limit, the phase and amplitude response are governed by the Fabry–Pérot transmission equation (equation (1)) [28]. The complex transmission amplitude (t_{FP}) is then given as,

$$t_{\text{FP}} = \frac{4\,(n_{\text{eff}}/n_0)\,\mathrm{e}^{\mathrm{i}n_{\text{eff}}k_0H}}{(n_{\text{eff}}/n_0+1)^2 - (n_{\text{eff}}/n_0-1)^2\,\mathrm{e}^{2\mathrm{i}\,n_{\text{eff}}k_0H}}, \tag{1}$$

where n_{eff} is the effective refractive index of the dominant mode, n_0 is the refractive index of background, k_0 is the wavenumber, and H is the height of the resonator. The phase shift would correspond to $\arg(t_{\text{FP}})$, and the transmission to $|t_{\text{FP}}|$. The effective refractive index (n_{eff}) is extracted from a mode analysis performed with the Lumerical MODE Solver (supplementary figure S1). The theoretical phase map from equation (1) (figure 3(b)) matches the numerical results (figure 3(a)) to within 0.1 rad (supplementary figures S2 and S3) confirming that each metaatom behaves as a Fabry–Pérot–type resonator. Notably, the full 2π phase swing arises from a resonance that spans the $60\lambda_{\text{Si}}$-long modified region, and because the lateral pitch (300–500 nm) is $\leqslant\lambda_{\text{Si}}$, the higher diffraction orders are suppressed. Every metaatom therefore effectively behaves as a single-mode slab whose phase fully characterized by a single n_{eff}, eliminating spurious beams

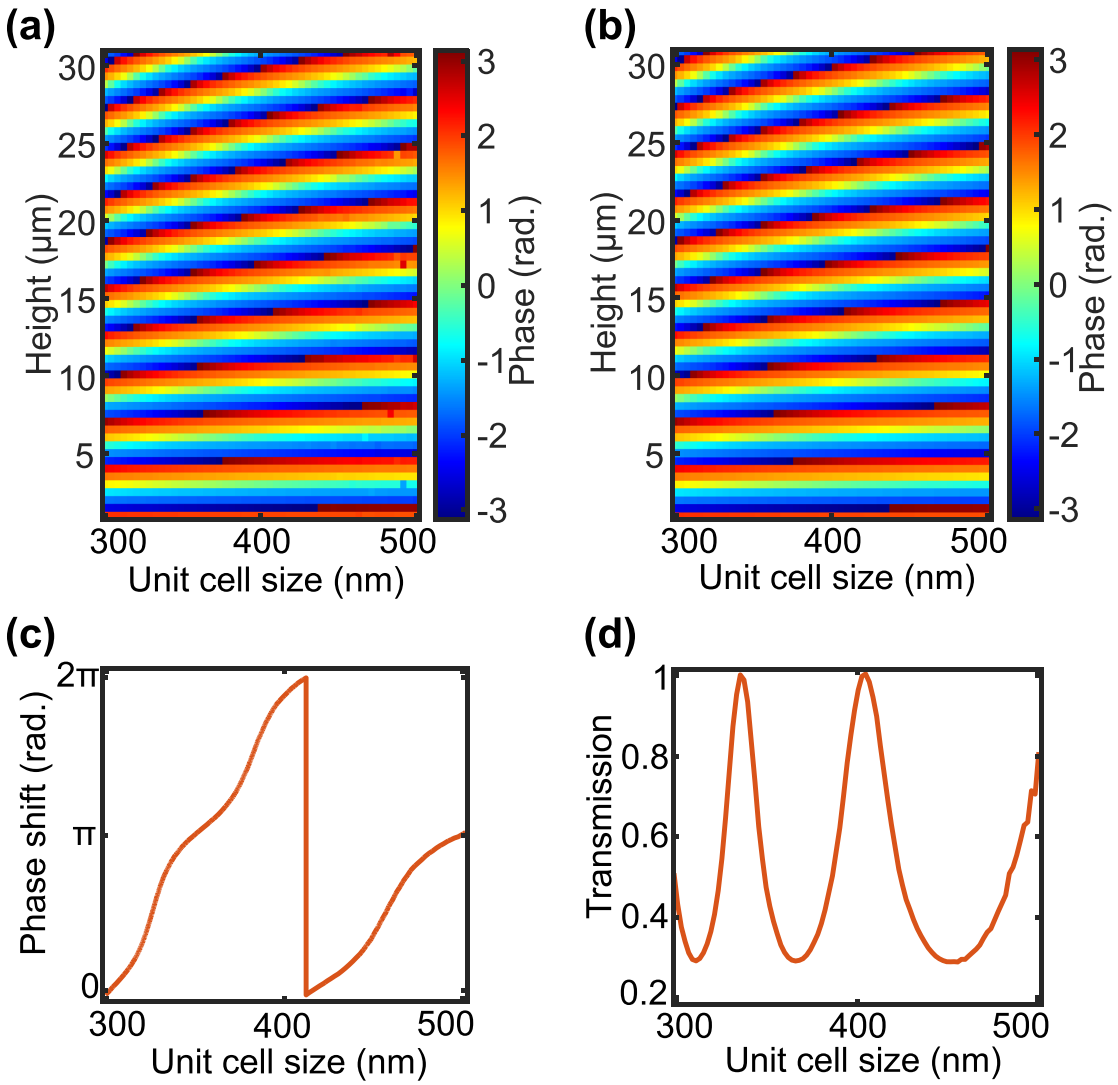

Figure 3. Numerical and semi-analytical analyses of metaatoms for $\Delta n = 0.25$. (a) FDTD simulation of phase shift for 300–500 nm unit cell size and 0–30 μm heights. (b) Semi-analytical estimate from equation (1). We assume $60 \times \lambda_{Si}$ for the modification and substrate height in (a) and (b). (c) FDTD simulation of phase shift for $H_{modif} = 60 \times \lambda_{Si}$ and $H_{sub} = 80 \times \lambda_{Si}$ fully buried subsurface metaatoms. (d) FDTD simulation of transmission under normal incidence.

and ensuring that the collective phase response is dictated by subwavelength resonant coupling rather than simple geometric path length [28].

4. Metalens design for continuous nanofabrication

We design the metalens with the hyperbolic phase profile, $\varphi(r,\theta) = 2\pi/\lambda\left(f - \sqrt{f^2 + r^2}\right)$, where λ is the operating wavelength, f the focal length, and (r, θ) the polar coordinates in the lens plane. Figure 4(a) shows the wrapped phase along the x-axis for a representative design with $f = 120\,\mu$m and an aperture diameter of 100 μm. By using the metaatom response given in figure 3(c), this phase profile is mapped to a unit cell distribution which in turn enables discretization (figure 4(b)). This step converts the ideal phase map into a layout that can be written as a continuous, laser-inscribed array. Although the numerical discretization is performed with few nanometer-level pitch increments for accuracy, the resulting phase map may be quantized to the granularity of experiments.

An important design consideration is the polarization response of metaatoms. The procedure described in figure 4(b) assumes an incident polarization angle of $\theta = 0°$, with the metaatom width δl oriented perpendicular to the polarization. Since the mapping procedure is a function of θ (supplementary figure S4), the preceding analysis can be repeated for the orthogonal case, $\theta = 90°$. A continuous, polarization-dependent phase profile is then obtained by fitting an elliptical interpolation curve in θ for each

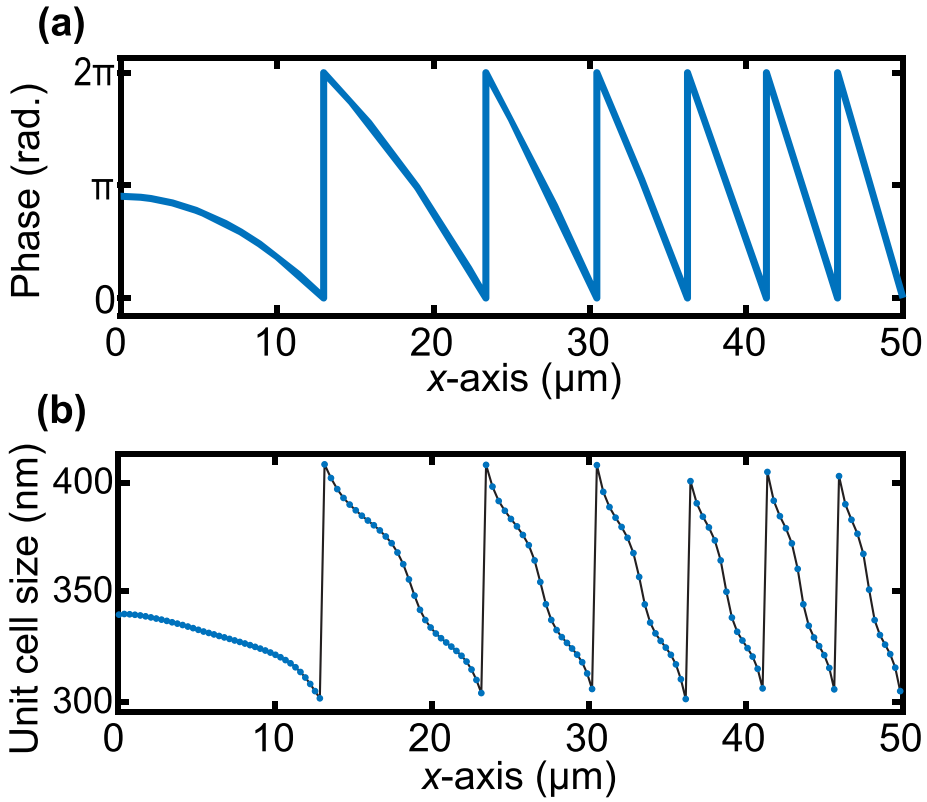

Figure 4. Phase mapping and discretization for the metalens. (a) The target phase along the x axis, found from the lens phase equation for $\varphi(r, \theta)$. (b) The phase is mapped to a unit cell distribution between 300 and 410 nm, computed with discretizing by ∼40 steps.

Δr_i. Due to the slow variation of phase with orientation, this construction captures the anisotropic phase response with high fidelity. The resulting loci in the (r, θ) plane are only slightly elliptical and merge smoothly (figure 2(c)), so the output phase of the metalens remains effectively circularly symmetric.

The complete metalens was simulated using a Lumerical 3D FDTD solver. The details of 3D FDTD simulations are given in the supplementary methods section. The resulting phase output closely matches the designed hyperbolic profile (figure 5(a)), and the simulations confirm effective focusing behavior (figures 5(b)–(d)). We obtain a promising focusing efficiency of 70% and a total transmission of 72%. All transmission and focusing efficiency simulations assume ideal anti-reflection coatings at the input and output interfaces.

5. Discussion

To our knowledge, this study presents the first blueprint for subsurface metaoptics, achieving high efficiency through subwavelength phase control. Laser-written metaatoms were analyzed using a combination of FDTD simulations and a semi-analytical model to characterize their phase response. These results guided the design of a volumetric metalens architecture. The resonant configuration enables full 2π phase modulation within a compact lateral footprint, supports fine phase quantization, and inherently suppresses the parasitic diffraction orders, features that distinguish it from non-resonant, path-length-based approaches. Experimental realizations will require precise and concurrent control over multiple fabrication parameters, including feature dimension, pitch, structure height, surface roughness, and refractive index modulation. While fine control over each parameter has been individually demonstrated in previous laser-writing studies [2, 3, 17], device implementations will demand simultaneous, high-fidelity control within a single workflow.

A critical direction for advancing this platform is refractive index engineering. The proposed architecture assumes localized amorphization within Si. Although full amorphization has not yet been achieved, recent ultrafast-laser writing studies report significant subsurface amorphization at the 100 nm scale [38]. Moreover, structural analyses of laser-modified regions reveal the formation of nanoscale voids [17], suggesting the possibility of achieving an index contrast as high as 2.5. These developments open a broad

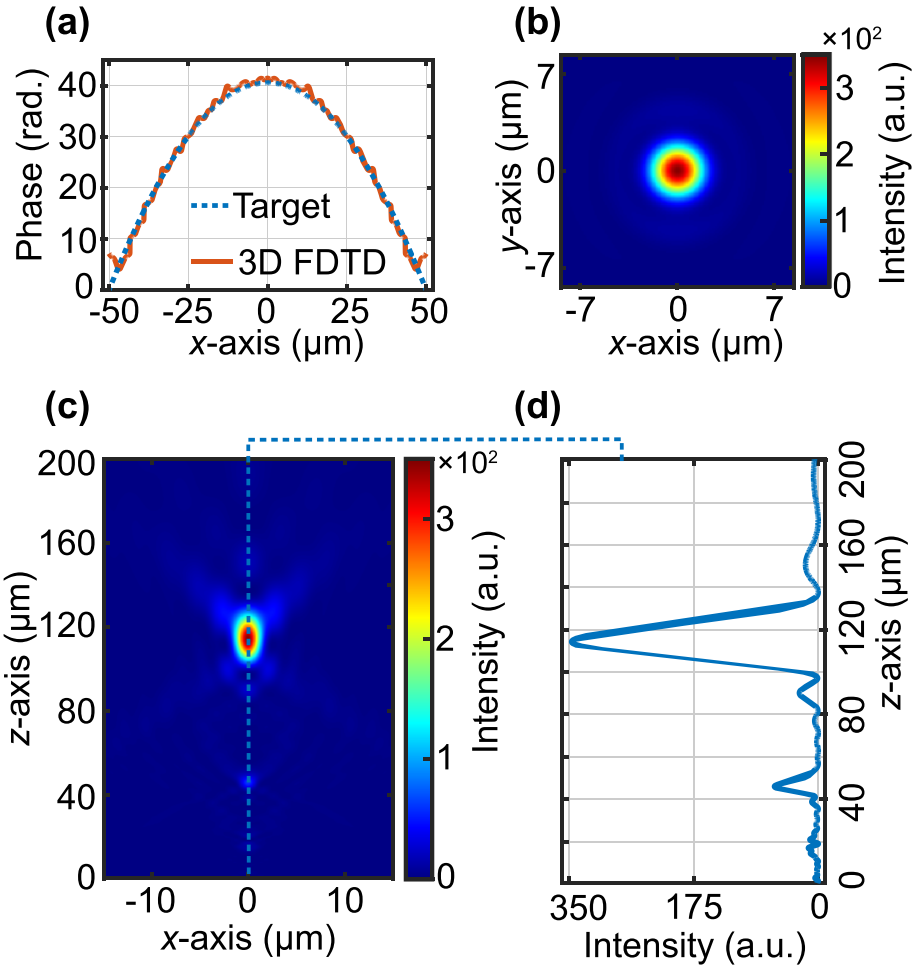

Figure 5. In-chip metalens numerical characterization. (a) Target phase front for a lens of $f = 120\ \mu$m and aperture size 100 μm, compared with the output (3D FDTD) of the designed element. (b) Intensity profile at the focal plane. (c) Propagation of the field in the x–z plane. The metalens is positioned at $z = 0$. (d) The $x = 0$ cross-section of the field intensity after the metalens. Electric field is polarized along the x-axis. Total simulation time of the metalens was near 1000 h on a computer with Intel i7-10 700 F processor.

design space for buried, high-performance metaoptics. Even the existing index contrast of $|\Delta n| \approx 10^{-2}$, as previously reported [17], may be sufficient. FDTD simulations in the 300−500 nm unit cell size range confirm that full 2π phase modulation can be achieved (supplementary figure S5). In this regime, the reduced coupling strength is compensated by increasing the metaatom length up to $1200\lambda_{Si}$, or approximately half a millimeter (table S1). Although maintaining alignment over such aspect ratios is challenging, high-aspect-ratio structuring has already been demonstrated inside Si [3].

Device performance may be sensitive to fabrication imperfections, including variations in metaatom height, feature size, unit cell pitch, and refractive index. To assess robustness, we performed Monte Carlo simulations to evaluate phase sensitivity to these parameters (table S2). The results indicate a fabrication-tolerant phase error of ≈0.5 radians. Minimizing scattering losses requires sidewall roughness below $\lambda_{Si}/30$ [28, 43]. Encouragingly, state-of-the-art laser-written modifications in Si have achieved sidewall roughness near $\lambda_{Si}/40$, which is promising for nanophotonic applications [17]. Comparable tolerances apply to pitch and feature dimensions in current in-chip nano-fabrication [17].

The current architecture encodes phase through unit cell size, discretized into forty levels (figure 4(b)). Even a binary palette can produce a functional metalens, albeit with reduced efficiency [44]. Existing laser writing systems can generate five distinct levels, and further advances are anticipated to push this figure higher. Future efforts should aim to concurrently meet fabrication tolerances, sub−30 nm accuracy in height and pitch, sidewall roughness below $\lambda_{Si}/30$, and unit cell quantization finer than today's five-level benchmark. These targets are within reach of current capabilities, and further improvements in beam shaping, feedback metrology, and post-polish planarization may help close the remaining gap.

6. Conclusion

We have demonstrated subwavelength phase engineering deep inside crystalline Si by leveraging 3D laser writing and buried high-aspect-ratio metaatoms. Extensive FDTD simulations, supported by a semi-analytical Fabry–Pérot model, reveal that arrays of 250 nm-wide metaatoms can provide full 0–2π phase coverage at $\lambda = 1.55$ μm with single-metaatom transmission up to 90%. Using such building blocks, we designed a 100 μm-aperture metalens with a simulated focusing efficiency of 70%. Recent progress in direct laser-nanofabrication, refractive index engineering and observations of localized amorphization and nanovoid formation in Si point to an emerging design space. These also highlight fabrication challenges for nanosecond and ultrafast laser nanofabrication. In particular, precise refractive index engineering needs to be achieved along with realization of sub−30 nm accuracy in height, pitch, and roughness values. Continued progress in beam shaping, adaptive feedback metrology, and multi-beam writing approaches are expected to surmount these challenges and exploit the depth degree of freedom for buried nanophotonics.

Future research aimed at fully 3D nanophotonic elements could unlock improved functionality, broadband operation and highly compact footprints. Ultimately, the 3D Si-metaoptics paradigm holds the promise of multi-level monolithic integration for diverse functionalities. The maskless fabrication offers a direct, scalable and cost-effective path to buried subwavelength optics, devices that could operate alongside surface elements within standard CMOS flows, such as electronics, MEMS/NEMS, and conventional metasurfaces [17]. Given Si's transparency in the near- and mid-infrared, the platform can naturally extend to longer wavelengths. If fully 3D nanoscale architectures become accessible, one can also envision spatial multiplexing of optical functionality [45, 46]. Together, these developments chart a course toward wafer-scale, volumetric photonic integration that unites advanced optical functionality with the maturity and industrial reach of the Si platform. We further anticipate that the subwavelength optical engineering will translate to other transparent media, particularly in light of recent advances in ultrafast laser nanostructuring of glasses and wide-bandgap dielectrics [8, 47–49].

Data availability statement

All data that support the findings of this study are included within the article (and any supplementary files).

Acknowledgment

This study was partially supported by The Scientific and Technological Research Council of Turkey (TUBITAK) (Project No: 123M873, 123C530).

Conflict of interest

The authors have no conflict of interest.

ORCID iDs

Mehmet Bütün 0000-0002-2058-2971
Alperen Saltik 0009-0008-5654-3713
Onur Tokel 0000-0003-1586-4349

References

[1] Staude I and Schilling J 2017 Metamaterial-inspired silicon nanophotonics *Nat. Photon.* **11** 274–84
[2] Chambonneau M *et al* 2021 In-volume laser direct writing of silicon—challenges and opportunities *Laser Photon. Rev.* **15** 2100140
[3] Tokel O *et al* 2017 In-chip microstructures and photonic devices fabricated by nonlinear laser lithography deep inside silicon *Nat. Photon.* **11** 639–45
[4] Tauseef M A, Asgari Sabet R and Tokel O 2024 Laser lithography of monolithically-integrated multi-level microchannels in silicon *Adv. Mater. Technol.* **9** 2301617
[5] Saltik A and Tokel O 2024 Laser-written wave plates inside the silicon enabled by stress-induced birefringence *Opt. Lett.* **49** 49–52
[6] Ródenas A *et al* 2019 Three-dimensional femtosecond laser nanolithography of crystals *Nat. Photon.* **13** 105–9
[7] Xu X *et al* 2022 Femtosecond laser writing of lithium niobate ferroelectric nanodomains *Nature* **609** 496–501
[8] Li Z *et al* 2024 Super-stealth dicing of transparent solids with nanometric precision *Nat. Photon.* **18** 799–808
[9] Turnali A, Han M and Tokel O 2019 Laser-written depressed-cladding waveguides deep inside bulk silicon *J. Opt. Soc. Am. B* **36** 966–70
[10] Matthäus G *et al* 2018 Inscription of silicon waveguides using picosecond pulses *Opt. Express* **26** 24089–97
[11] Chanal M *et al* 2017 Crossing the threshold of ultrafast laser writing in bulk silicon *Nat. Commun.* **8** 773
[12] Chambonneau M, Richter D, Nolte S and Grojo D 2018 Inscribing diffraction gratings in bulk silicon with nanosecond laser pulses *Opt. Lett.* **43** 6069–72

[13] Wang X et al 2021 Curved waveguides in silicon written by a shaped laser beam Opt. Express 29 14201–7
[14] Alberucci A et al 2020 In-depth optical characterization of femtosecond-written waveguides in silicon Phys. Rev. Appl. 14 024078
[15] Bütün M, Saylan S, Asgari Sabet R and Tokel O 2023 High-efficiency multilevel volume diffraction gratings inside silicon ACS Mater. Au 3 727–33
[16] Tokel O et al 2014 Laser-writing in silicon for 3D information processing (arXiv:1409.2827v1)
[17] Asgari Sabet R, Ishraq A, Saltik A, Bütün M and Tokel O 2024 Laser nanofabrication inside silicon with spatial beam modulation and anisotropic seeding Nat. Commun. 15 5786
[18] Chen H, Taylor A J and Yu N 2016 A review of metasurfaces: physics and applications Rep. Prog. Phys. 79 076401
[19] Kuznetsov A I et al 2024 Roadmap for optical metasurfaces ACS Photon. 11 816–65
[20] Shelby R A, Smith D R and Schultz S 2001 Experimental verification of a negative index of refraction Science 292 77–79
[21] Roques-Carmes C et al 2022 Toward 3D-printed inverse-designed metaoptics ACS Photon. 9 43–51
[22] Li A, Singh S and Sievenpiper D 2018 Metasurfaces and their applications Nanophotonics 7 989–1011
[23] Quevedo-Teruel O et al 2019 Roadmap on metasurfaces J. Opt. 21 073002
[24] Jahani S and Jacob Z 2016 All-dielectric metamaterials Nat. Nanotechnol. 11 23–36
[25] Zhou Y et al 2018 Multilayer noninteracting dielectric metasurfaces for multiwavelength metaoptics Nano Lett. 18 7529–37
[26] Adi W et al 2024 Trapping light in air with membrane metasurfaces for vibrational strong coupling Nat. Commun. 15 10049
[27] Yu N et al 2011 Light propagation with phase discontinuities: generalized laws of reflection and refraction Science 334 333–7
[28] Lim S W D, Meretska M L and Capasso F 2021 A high aspect ratio inverse-designed holey metalens Nano Lett. 21 8642–9
[29] Chen W T, Zhu A Y and Capasso F 2020 Flat optics with dispersion-engineered metasurfaces Nat. Rev. Mater. 5 604–20
[30] Genevet P, Capasso F, Aieta F, Khorasaninejad M and Devlin R 2017 Recent advances in planar optics: from plasmonic to dielectric metasurfaces Optica 4 139–52
[31] Ji J et al 2024 On-chip multifunctional metasurfaces with full-parametric multiplexed Jones matrix Nat. Commun. 15 8271
[32] Zhou Y and Fan J A 2023 Polychromatic metasurfaces for complete control of phase and polarization in the mid-infrared Light Sci. Appl. 12 249
[33] Ishii S, Shalaev V M and Kildishev A V 2013 Holey-metal lenses: sieving single modes with proper phases Nano Lett. 13 159–63
[34] Yu N and Capasso F 2014 Flat optics with designer metasurfaces Nat. Mater. 13 139–50
[35] Gao S, Park C, Lee S and Choi D 2019 A highly efficient bifunctional dielectric metasurface enabling polarization-tuned focusing and deflection for visible light Adv. Opt. Mater. 7 1801337
[36] Wang X et al 2024 Direct observation and quantification of nanosecond laser induced amorphization inside silicon J. Laser Appl. 36 022015
[37] De Dood M, Polman A, Zijlstra T and Van der Drift E 2002 Amorphous silicon waveguides for microphotonics J. Appl. Phys. 92 649–53
[38] Grojo D et al 2024 In-chip critical plasma seeds for laser writing of reconfigurable silicon photonics systems (available at: https://hal.science/hal-04727973)
[39] Pavlov I et al 2017 Femtosecond laser written waveguides deep inside silicon Opt. Lett. 42 3028–31
[40] Blothe M, Alberucci A, Alasgarzade N, Chambonneau M and Nolte S 2024 Transverse inscription of silicon waveguides by picosecond laser pulses Laser Photon. Rev. 18 2400535
[41] Chambonneau M, Li Q, Chanal M, Sanner N and Grojo D 2016 Writing waveguides inside monolithic crystalline silicon with nanosecond laser pulses Opt. Lett. 41 4875–8
[42] Engelberg J and Levy U 2020 The advantages of metalenses over diffractive lenses Nat. Commun. 11 1991
[43] Ma X, He W, Xin L, Yang Z and Liu Z 2021 Imaging performance of a mid-infrared metalens with a machining error Appl. Opt. 61 60–68
[44] Hu Z, Yang Y, Xu L, Hao Y and Chen H 2022 Binary acoustic metasurfaces for dynamic focusing of transcranial ultrasound Front. Neurosci. 16 984953
[45] Hu J et al 2024 Diffractive optical computing in free space Nat. Commun. 15 1525
[46] Abdollahramezani S, Hemmatyar O and Adibi A 2020 Meta-optics for spatial optical analog computing Nanophotonics 9 4075–95
[47] Xu K et al 2025 All-glass nanohole metalens by non-diffracting laser lithography Laser Photon. Rev. 19 2402006
[48] Datta S, Clady R, Grojo D, Utéza O and Sanner N 2024 Scalable nanophotonic structures inside silica glass laser-machined by intense shaped beams Laser Photon. Rev. 18 2301365
[49] Gribaudo E, Deckart M, Vlugter P and Bellouard Y 2025 Sub-wavelength femtosecond laser based nanostructuring of complex patterns in the bulk of fused silica Opt. Express 33 11529–40